Received: 5 March 2024 | Revised: 4 May 2024 | Accepted: 13 May 2024

DOI: 10.1111/jace.19942

Journal of the American Ceramic Society

RESEARCH ARTICLE

Structural phase transitions in multicomponent $La_{0.2}Nd_{0.2}Sm_{0.2}Gd_{0.2}RE5_{0.2}NbO_4$ (RE5 = Ho, Y, Tb, Eu, Pr) oxides

Arkadiusz Dawczak | **Aleksandra Mielewczyk-Gryń** | **Maria Gazda**

Institute of Nanotechnology and Materials Engineering, and Advanced Materials Centre, Gdańsk University of Technology, Gdańsk, Poland

Correspondence
Arkadiusz Dawczak, Institute of Nanotechnology and Materials Engineering, and Advanced Materials Centre, Gdańsk University of Technology, 11/12 Gabriela Narutowicza, 80-233 Gdańsk, Poland.
Email: arkadiusz.dawczak@pg.edu.pl

Funding information
National Science Centre Poland, Grant/Award Number: 2019/35/B/ST5/00888; CERIC-ERIC, Grant/Award Number: 20212021

Abstract

In this work, the influence of compositional complexity on the structural and thermal properties of multicomponent rare-earth ortho-niobates from the $La_{0.2}Nd_{0.2}Sm_{0.2}Gd_{0.2}RE5_{0.2}NbO_4$ (RE5 = Ho, Y, Tb, Eu, Pr) series was investigated. Based on X-ray powder diffraction studies using synchrotron radiation, it was found that all tested materials were pure single-phase compositions and showed stability in the monoclinic I2/c crystal structure at room temperature. High-temperature X-ray powder diffraction studies and dilatometry studies confirmed the presence of a structural phase transition between low-temperature (I2/c) and high-temperature ($I4_1/a$) polymorphs. The structural phase transition temperatures are between 676°C and 701°C. Interestingly, despite their compositional complexity, the structural phase transition temperature behaves similarly to conventional ortho-niobates, that is, it depends on the radius of the A-cation; that is, as the ionic radius increases, the phase transition temperature decreases. The transition has been categorized as a second-order phase transition based on the observed relationship between the Landau order parameter and spontaneous strain. The coexistence of the tetragonal and monoclinic phases has been seen in all compositions around the temperature of the structural phase transition. The presence of two orientation states in the monoclinic structure leads to the so-called spontaneous strain, which consists of longitudinal (u) and shear (v) strain components. The values of these strains at 300°C range between 2.42 and 2.58×10^{-2} for longitudinal, 2.98 and 3.04×10^{-2} for shear, and 5.46 and 5.57×10^{-2} for scalar spontaneous strain. It was found that the spontaneous strain in each of the materials under test was very little impacted by the variation in the complexity of the A sublattice's composition. In addition, thermal expansion coefficients of both polymorphs were determined, which range from 12.7×10^{-6} K^{-1} to 13.2×10^{-6} K^{-1} for the monoclinic structure and 9.7×10^{-6} K^{-1} to 9.9×10^{-6} K^{-1} for the tetragonal one.

KEYWORDS
multicomponent oxides, rare-earth ortho-niobates, scalar spontaneous strain, structural phase transition

1 | INTRODUCTION

Rare-earth ortho-niobates are an interesting group of materials due to their potential use in electrochemical devices.[1–5] They exhibit interesting structural, thermal, and electrical properties. For example, they undergo the structural phase transition between the monoclinic and tetragonal structure,[6] hydrate in a wide temperature range,[7] and are ionic conductors.[8,9] Their properties can be modified by the substitution in a given sublattice. By doping the A sublattice with an acceptor-type ion, the ionic conductivity can be increased,[9] while by doping the B sublattice, the phase transition temperature can be lowered[10–12] or increased.[13] Nearly 20 years ago, Yeh et al.[14] presented a new concept of creating new materials—high-entropy materials. Initially, this concerned metal alloys, but since 2015, when Rost et al.[15] synthesized the first high-entropy oxide material (HEO), and scientists began developing new HEOs from other groups, such as ABO_3[16–18] and ABO_4.[19,20] By mixing different elements of different properties, one can obtain a new material with unknown properties, thanks to which we can, for example, improve its three key properties at the same time. So far, only one work has been reported on structural phase transitions in multicomponent rare-earth ortho-niobates.[21] In that work, the authors compared $La_{1/3}Nd_{1/3}Sm_{1/3}NbO_4$, $La_{1/4}Nd_{1/4}Sm_{1/4}Ho_{1/4}NbO_4$, and $La_{1/5}Nd_{1/5}Sm_{1/5}Ho_{1/5}Y_{1/5}NbO_4$ and found that the temperature of structural phase transition in $La_{1/5}Nd_{1/5}Sm_{1/5}Ho_{1/5}Y_{1/5}NbO_4$ is 700°C, which is 160°C higher than that in undoped $LaNbO_4$.[21] They explained this as related to the size of the RE constituents.

In this work, we present the results of synchrotron radiation X-ray diffraction (SR-XRD), spontaneous strains and Landau order parameters of the $La_{0.2}Nd_{0.2}Sm_{0.2}Gd_{0.2}RE5_{0.2}NbO_4$ (where RE5 = Ho, Y, Tb, Eu, Pr) series. Additionally, phase transition temperatures (T_0) and thermal expansion coefficients (TECs) of the above-mentioned compounds were determined through dilatometric measurements.

2 | EXPERIMENTAL

The $La_{0.2}Nd_{0.2}Sm_{0.2}Gd_{0.2}Ho_{0.2}NbO_4$, $La_{0.2}Nd_{0.2}Sm_{0.2}Gd_{0.2}Y_{0.2}NbO_4$, $La_{0.2}Nd_{0.2}Sm_{0.2}Gd_{0.2}Tb_{0.2}NbO_4$, $La_{0.2}Nd_{0.2}Sm_{0.2}Gd_{0.2}Eu_{0.2}NbO_4$, and $La_{0.2}Nd_{0.2}Sm_{0.2}Gd_{0.2}Pr_{0.2}NbO_4$ materials were prepared by a three-stage solid state route using La_2O_3 (Chempur 99.99%), Nd_2O_3 (Chempur 99.9%), Sm_2O_3 (Chempur 99.9%), Gd_2O_3 (Chempur 99.9%), Ho_2O_3 (Chempur 99.9%), Y_2O_3 (Chempur 99.99%), Tb_4O_7 (Alfa Aesar 99.9%), Eu_2O_3 (Chempur 99.9%), Pr_6O_{11} (Arcos Organics 99.9%), and Nb_2O_5 (Alfa Aesar 99.9%) as starting reagents. Because of their hygroscopicity, the lanthanum and neodymium oxides were annealed in a furnace at 900°C for 12 h before being weighed for the first synthesis stage. To maintain the repeatability of the synthesis process and thus the possibility of comparing their properties, the materials were prepared in the same way as described in our previous work.[20] That is, the materials were synthesized using a three-step solid-state synthesis method, starting from the preparation of a stoichiometric mixture of reagents, which was ground in an agate mortar with the addition of isopropyl alcohol. Then, the powders were heated at a temperature of 750°C (with a heating and cooling rate of 5°C min^{-1}) for 24 h. In the next step, the powders were ground again, sieved through a 100 μm sieve, uniaxially compressed under a pressure of 250 MPa and sintered at a temperature of 1400°C (at a heating and cooling rate of 2°C min^{-1}) for 12 h. In the final stage, which was similar to the second stage, the prepared pellets were sintered at a temperature of 1500°C (with a heating and cooling rate of 2°C min^{-1}) for 12 h to obtain dense samples.

The SR-XRD experiment was performed at the MCX beamline (Elletra) at a wavelength of λ = 0.688801 Å (energy range 18 keV) in a transmission geometry using a point fast scintillator detector. The measurements were carried out on powder samples at room temperature.

X-ray powder diffraction (XRD) measurements were carried out using $Cu_{K\alpha}$ radiation on a Philipps X'Pert Pro diffractometer in the 2θ range 15°–130° and a temperature range from room temperature to 850°C. Measurements at temperatures above room temperature were performed using a high-temperature Anthon Paar HT-1200 oven adapter. The phase composition was determined using HighScore Plus Analysis software.[22] The crystal structure of the samples was refined using Rietveld analysis with GSAS-II software.[23] Structural data presented in our previous work were used for refinement.[20] A separate CIF file was prepared for each compound using the VESTA software,[24] and then uploaded to the GSAS-II program. For the analysis in which only one of the polymorphic varieties of the compound occurred, appropriate assumptions

were used in the program, such as the assumption that five different elements occupy the same position in the crystal lattice (constrains, make atoms equivalent). However, if the analysis was performed in an area close to the coexistence of two phases, an additional limitation was introduced in the program because it is possible to determine the percentage share of a given phase (histogram, phase fraction). Low-temperature Fergusonite-type I2/c (no. 15) and high-temperature Scheelite-type $I4_1/a$ (no. 88) crystal structures were utilized as a starting point for the analysis.[6,25] Dilatometry measurements were carried out using a Netzsch 402 PC/4 device. Dense rectangular samples ($15 \times 5 \times 2.5$ mm^3) were used. The density of the examined materials was calculated using the vacuum-assisted Archimedes technique. All collected samples had a density of 93%–98% of the theoretical density. The synthetic dry air (50 mL min^{-1}) was used for the measurements, which were done between 50°C and 1000°C at a heating/cooling rate of 2°C min^{-1}.

Lanthanum ortho-niobate undergoes the structural phase transition from the monoclinic (low temperature, I2/c) to tetragonal (high temperature, $I4_1/a$) crystal structure which is usually described as the second-order transition.[6,25] The tetragonal phase is paraelastic, and the monoclinic phase is ferroelastic, in which two different orientation states exist.[6] The presence of two orientation states leads to so-called spontaneous strain. To determine the values of the strain tensor components and the scalar spontaneous strain, the theory of ferroelastic materials presented by Aizu[26] relating strain to the parameters of the unit cell introduced by Schlenker et al.[27] will be applied. The spontaneous strain tensor of Aizu $\varepsilon_s(S_i)$ is expressed by Equation (1). It assumes that $\varepsilon_s(S_i)$ represents the strain tensor in a particular state S_i, and S_1, S_2, …, S_q are all orientation states of the ferroelastic crystal.[6]

$$\varepsilon_s(S_i) = \varepsilon(S_i) - \frac{1}{q}\sum_{k=1}^{q}\varepsilon(S_k) \tag{1}$$

which defines the spontaneous strain ε_s by the following equation (Equation 2).

$$\varepsilon_s^2 = \sum_{i=1}^{3}\sum_{j=1}^{3}\varepsilon_{sij}^2 \tag{2}$$

where $\varepsilon_{sij} = \varepsilon(S_i) - \frac{1}{q}\varepsilon(S_j)$ is the ij component of the $\varepsilon_s(S_k)$ tensor.

Because in the Fergusonite structure there are only two (S_1 and S_2) orientations, the strain components and the relations between them are described by Equations (3)–(7).

$$\varepsilon_{11} = \frac{c_m \sin\beta_m}{a_t} - 1 \tag{3}$$

$$\varepsilon_{22} = \frac{a_m}{a_t} - 1 \tag{4}$$

$$\varepsilon_{33} = \frac{b_m}{c_t} - 1 \tag{5}$$

$$\varepsilon_{12} = \varepsilon_{21} = -\frac{c_m \cos\beta_m}{2a_t} \tag{6}$$

$$\varepsilon_{13} = \varepsilon_{31} = \varepsilon_{23} = \varepsilon_{32} = 0 \tag{7}$$

where a_m, b_m, c_m, and β_m are lattice parameters of the monoclinic phase and a_t and c_t are those of the tetragonal phase. Equations (8) and (9) describe the strain tensors.

$$\varepsilon(S_1) = \begin{pmatrix} \varepsilon_{11} & \varepsilon_{21} & 0 \\ \varepsilon_{12} & \varepsilon_{22} & 0 \\ 0 & 0 & \varepsilon_{33} \end{pmatrix} \tag{8}$$

$$\varepsilon(S_2) = R\varepsilon(S_1)R^T \tag{9}$$

where R is the 90° rotation matrix and R^T is the transpose of R.

Equations (10)–(13) show the spontaneous strain tensors (1) modified by Aizu.

$$\varepsilon_s(S_1) = \begin{pmatrix} -u & v & 0 \\ v & u & 0 \\ 0 & 0 & 0 \end{pmatrix} \tag{10}$$

$$\varepsilon_s(S_2) = \begin{pmatrix} u & -v & 0 \\ -v & -u & 0 \\ 0 & 0 & 0 \end{pmatrix} \tag{11}$$

$$u = \frac{1}{2}(\varepsilon_{22} - \varepsilon_{11}) \tag{12}$$

$$v = \varepsilon_{12} \tag{13}$$

where u and v are the longitudinal and shear spontaneous strain components, respectively. The data obtained from the Rietveld analysis will be used for further calculations. The magnitude of scalar spontaneous strain is given as (Equation 14):

$$\varepsilon_s^2 = 2\left(u^2 + v^2\right) \tag{14}$$

Assuming that the Fergusonite–Scheelite transition is of the second order, it may be described using the so-called Landau order parameter, η (Equation 15). It is equal to zero at and above the critical temperature of the phase transition (T_0) and increases continuously with decreasing

temperature.

$$\eta = \left[\frac{T_0 - T}{T}\right]^{\frac{1}{2}} \quad (15)$$

The relationship between the order parameter and the spontaneous strain in the lanthanum ortho-niobate system is linear which is described by the following equation (Equation 16).

$$\eta = k\varepsilon_s \quad (16)$$

3 | RESULTS AND DISCUSSION

3.1 | Synchrotron radiation X-ray diffraction

Figure 1 shows the SR-XRD patterns of $La_{0.2}Nd_{0.2}Sm_{0.2}Gd_{0.2}RE5_{0.2}NbO_4$ (where RE5 = Ho, Y, Tb, Eu, and Pr) obtained at room temperature (Figure 1A) and exemplary Rietveld refinement profile (Figure 1B) of the $La_{0.2}Nd_{0.2}Sm_{0.2}Gd_{0.2}Ho_{0.2}NbO_4$ sample. The Rietveld refinement profiles of the other samples can be found in Figure S1a–d. All observed reflections indicate that the synthesized samples are pure single-phase materials with the monoclinic I2/c structure of the Fergusonite type. The unit cell parameters obtained based on the Rietveld analysis can be found in Table 1. For comparison, the calculated average values based on unit cell parameters of $LaNbO_4$,[28] $NdNbO_4$,[29] $SmNbO_4$,[30] $GdNbO_4$,[31] $HoNbO_4$,[30] $YNbO_4$,[32] $TbNbO_4$,[33] $EuNbO_4$,[34] and $PrNbO_4$[35] are also shown. It can be seen that the obtained unit cell parameters are similar to the corresponding average values. The differences are low; in particular, the *a*, *b*, and *c* parameters and unit cell volumes are slightly larger, while the

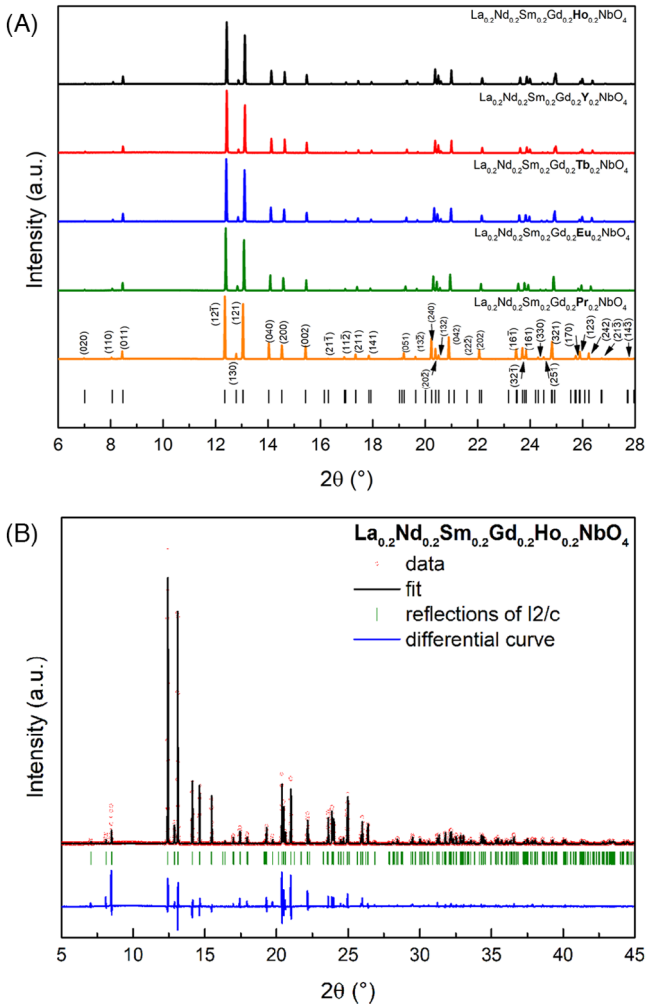

FIGURE 1 (A) Synchrotron radiation X-ray diffractograms of the $La_{0.2}Nd_{0.2}Sm_{0.2}Gd_{0.2}RE5_{0.2}NbO_4$ (RE5 = Ho, Y, Tb, Eu, Pr) series. Radiation of the 0.688801 Å wavelength was applied. (B) Rietveld profile of the pattern and difference plots for $La_{0.2}Nd_{0.2}Sm_{0.2}Gd_{0.2}Ho_{0.2}NbO_4$.

TABLE 1 Unit cell parameters, average radii of the A-site ions (r_A), and Rietveld analysis fit parameters of $La_{0.2}Nd_{0.2}Sm_{0.2}Gd_{0.2}RE_{0.2}NbO_4$ (RE = Ho, Y, Tb, Eu, Pr).

RE5	*a* (Å)	*b* (Å)	*c* (Å)	*β* (°)	*V* (Å^3)	r_A (Å)	GOF
Ho	5.43361 (8)	11.22497 (1)	5.13916 (7)	94.445 (8)	312.505 (3)	1.083	3.42
Ho[a]	5.424494	11.202926	5.127487	94.47908	310.8216	1.083	–
Y	5.43356 (2)	11.22566 (8)	5.13943 (1)	94.451 (9)	312.536 (1)	1.084	2.33
Y[a]	5.423212	11.201246	5.126365	94.46544	310.6464	1.084	–
Tb	5.44097 (9)	11.23448 (4)	5.13844 (8)	94.491 (9)	313.131 (4)	1.088	3.26
Tb[a]	5.434052	11.219106	5.130265	94.50664	311.9404	1.088	–
Eu	5.45076 (9)	11.25409 (1)	5.14399 (8)	94.485 (9)	314.584 (4)	1.093	3.57
Eu[a]	5.442592	11.236766	5.135105	94.49604	313.1951	1.093	–
Pr	5.47277 (7)	11.29829 (9)	5.15417 (6)	94.462 (7)	317.731 (3)	1.105	3.88
Pr[a]	5.463652	11.279506	5.144265	94.47744	316.1704	1.105	–

[a]The unit cell parameters calculated as an average of La-, Nd-, Sm-, Gd-, Ho-, Y-, Tb-, Eu-, and $PrNbO_4$ values are given for comparison.

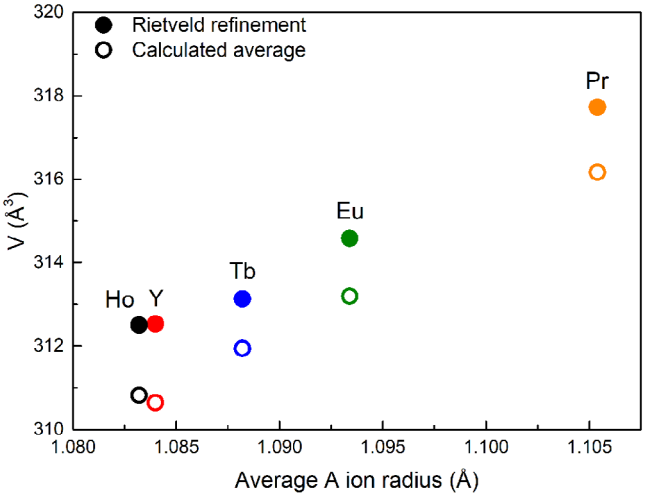

FIGURE 2 Unit cell volume as a function of the average ion radius of the A-cation in the $La_{0.2}Nd_{0.2}Sm_{0.2}Gd_{0.2}RE5_{0.2}NbO_4$ (RE = Ho, Y, Tb, Eu, Pr) series. Filled symbols represent the data obtained from the refinement, while the open ones correspond to the calculated averages.

monoclinic angles are slightly lower than the calculated ones. Unit cell parameters depend on the ionic radii of the constituents. Assuming that every ion inhabiting the A sublattice has the same coordination number (CN = 8), the average ionic radius (r_A) is the weighted average of its Shannon ionic radii.[36] The values for all studied oxides are shown in Table 1, while Figure 2 graphically shows the dependence of the volume of the unit cell on the average ionic radii of the A-cations. The unit cell volume (open symbols) monotonically increases with the increasing value of the average ionic radii. The calculated average values of the unit cell parameters show the same behavior (filled symbols); however, as mentioned above, their values are lower than the experimentally determined ones, with a relative difference between 0.4% and 0.6%. This may be related to the short-range disorder present in the multicomponent $La_{0.2}Nd_{0.2}Sm_{0.2}Gd_{0.2}RE5_{0.2}NbO_4$ oxides.

3.2 | High-temperature X-ray diffraction

Figure 3 presents the high-temperature X-ray diffractograms of $La_{0.2}Nd_{0.2}Sm_{0.2}Gd_{0.2}Ho_{0.2}NbO_4$ obtained at selected temperatures. Additionally, on the right-hand side, there is an enlargement in the angular range of 45°–50°, in which the diffraction reflections coming from the monoclinic structure get closer to each other as the temperature increases, where at 660°C, they merge. In Figure S2a–d, the high-temperature X-ray diffractograms for the other samples are presented. While the patterns correlate to the tetragonal body-centered Scheelite-type structure ($I4_1/a$) above 680°C, all of the reflections may be indexed in the monoclinic Fergusonite-type structure (I2/c) below 640°C. The Rietveld refinement results showed that at 620°C, there is 100% of the monoclinic phase, at 640°C and 660°C, the amount of the monoclinic phase is 91.1%, and 19.6 %, respectively, and at 680°C, there is only the tetragonal phase.

For all of the compounds, we observed the coexistence of the monoclinic and tetragonal phases near the structural phase transition temperature. The coexistence of two phases (monoclinic and tetragonal) near phase transition temperatures in rare-earth ortho-niobates has already been reported by many researchers.[11,28,29,33,37] For example, according to Arulnesan et al.[33] for $PrNbO_4$, the range of coexistence of two phases was 500°C–620°C. Saura-Múzquiz et al.[29] reported a range of 620°C–720°C for $NdNbO_4$. Our results show the coexistence of two phases in a relatively narrow temperature range, that is, 620°C–680°C for $La_{0.2}Nd_{0.2}Sm_{0.2}Gd_{0.2}Ho_{0.2}NbO_4$, 640°C–680°C for $La_{0.2}Nd_{0.2}Sm_{0.2}Gd_{0.2}Y_{0.2}NbO_4$, 620°C–660°C for $La_{0.2}Nd_{0.2}Sm_{0.2}Gd_{0.2}Tb_{0.2}NbO_4$, 620°C–660°C for $La_{0.2}Nd_{0.2}Sm_{0.2}Gd_{0.2}Eu_{0.2}NbO_4$, and 600°C–660°C for $La_{0.2}Nd_{0.2}Sm_{0.2}Gd_{0.2}Pr_{0.2}NbO_4$. Two possible explanations for the coexistence of two phases near the structural phase transition region were proposed by Sarin et al.[32] That is, either there is coupling between the order parameter and the residual strains in individual crystallites, or there is a range of particle sizes in the sample, where the surface energy of the smaller sized particles alters the relative stability of the two structures.[29]

3.2.1 | Unit cell parameters, spontaneous strain, and Landau order parameter

The unit cell parameters of the compounds were determined using the Rietveld analysis and are presented in Figure 4A–D as a function of temperature. In Figure 4A, it can be observed that with the increase in the temperature, the a_m and c_m unit cell parameters corresponding to the monoclinic I2/c crystal structure tend to one value, which corresponds to a_t axis of the tetragonal polymorph.

Temperature dependence of the unit cell parameters shows the evolution typical of the structural transition between the monoclinic and tetragonal structures.[37] The monoclinic β_m angle decreases from ~94.5° at room temperature to 90° at and above the transition temperature, as shown in Figure 4C. Also, the continuous transition between the a_m and c_m parameters and the a_t parameter (Figure 4A) as well as between b_m and the c_t parameter (Figure 4B) can be seen. Around the phase transition temperature (between 660°C and 680°C; depending on

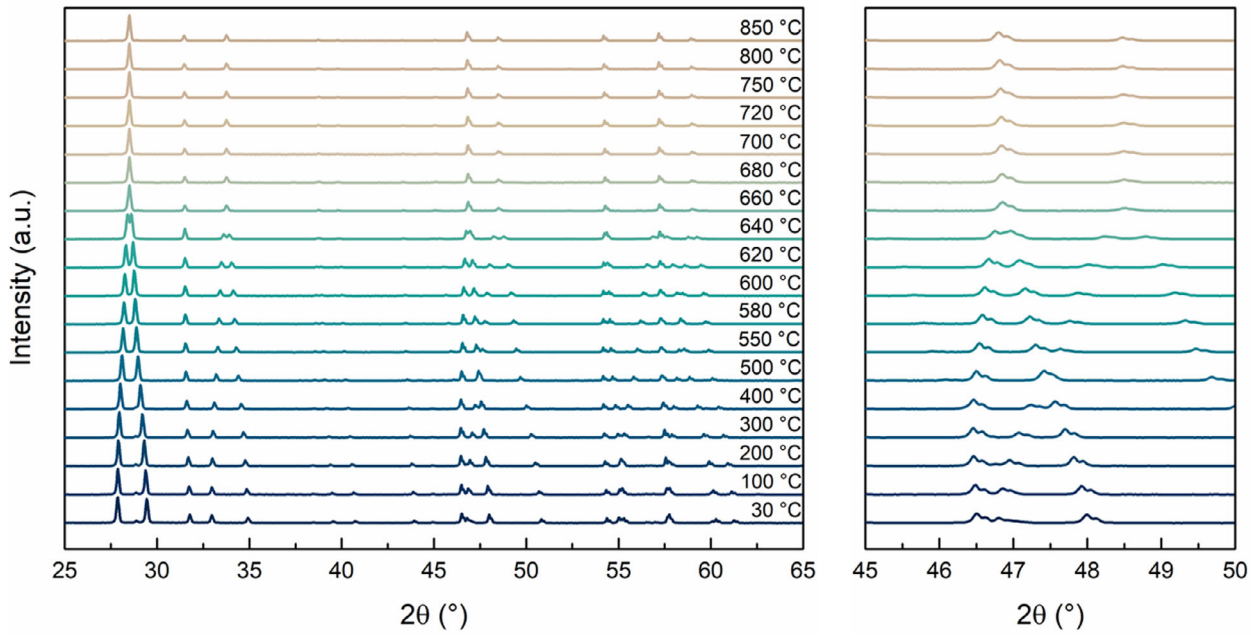

FIGURE 3 High-temperature X-ray diffraction patterns of the $La_{0.2}Nd_{0.2}Sm_{0.2}Gd_{0.2}Ho_{0.2}NbO_4$ collected at selected temperatures.

the composition), the plot of the temperature dependence of the unit cell volume (Figure 4D) displays a change in slope, which corresponds to a change in the TEC accompanying the structural phase transition. In Figure 5, to provide guidance for the eye, the changes in the unit cell shape and its crystallographic description during the structural phase transition from monoclinic to tetragonal and in reverse are presented. As demonstrated in Figure 5, the crystallographic nomenclature regarding the Fergusonite–Scheelite structural phase transition requires that the *c* axis of the tetragonal unit cell corresponds to the *b* axis of the monoclinic unit cell, whereas the *a* axis remain the same. Figure 6 shows the scalar spontaneous strain as a function of temperature (a) and order parameter η (b).

As can be seen, scalar spontaneous strain is equal to about 7×10^{-2} at room temperature and decreases to zero as the temperature increases up to the phase transition temperature. The values of longitudinal, shear and scalar spontaneous strain at 300°C, and the average constant *k* are listed in Table 2 for $La_{0.2}Nd_{0.2}Sm_{0.2}Gd_{0.2}Ho_{0.2}NbO_4$, $La_{0.2}Nd_{0.2}Sm_{0.2}Gd_{0.2}Y_{0.2}NbO_4$, $La_{0.2}Nd_{0.2}Sm_{0.2}Gd_{0.2}Tb_{0.2}NbO_4$, $La_{0.2}Nd_{0.2}Sm_{0.2}Gd_{0.2}Eu_{0.2}NbO_4$, and $La_{0.2}Nd_{0.2}Sm_{0.2}Gd_{0.2}Pr_{0.2}NbO_4$, respectively.

The values of longitudinal (u) components at 300°C increase with increasing average radius of the A ion. They are similar to the values presented in the literature, where for example, Jian and Wayman reported 2.878×10^{-2} for $LaNbO_4$.[6] Whereas Mielewczyk-Gryń et al. noted 2.37×10^{-2} for $La_{0.98}Mg_{0.02}NbO_{4-\delta}$ at 300°C.[37] The values of shear strain (v) except for those of $La_{0.2}Nd_{0.2}Sm_{0.2}Gd_{0.2}Pr_{0.2}NbO_4$ also increase with ionic radius. Praseodymium oxides easily absorb and desorb oxygen,[38,39] which may influence the strain observed at 300°C. The shear strain components are higher than those observed in $LaNbO_4$ and $La_{0.98}Mg_{0.02}NbO_{4-\delta}$[6,37] ($2.278 \times 10^{-2}$ and 1.49×10^{-2}, respectively). This originates from higher monoclinic angles found in $La_{0.2}Nd_{0.2}Sm_{0.2}Gd_{0.2}RE5_{0.2}NbO_4$ (at 300°C between 93.4° and 93.6°) than those in $LaNbO_4$ (93.0°) and $La_{0.98}Mg_{0.02}NbO_{4-\delta}$ (91.8°).[6,37] Higher shear strain components observed in the multicomponent ortho-niobates lead to higher scalar spontaneous strains in comparison to those in the undoped $LaNbO_4$ for which Jian and Wayman reported 5.199×10^{-2} at 300°C.[6] In addition, Mielewczyk-Gryń et al. for $La_{0.98}Mg_{0.02}NbO_{4-\delta}$ showed that the value of strain was 3.96×10^{-2} at 300°C.[37]

The structural phase transition between the monoclinic and tetragonal phases in most cases has been classified as a phase transition of the second order due to changes in the

TABLE 2 The values of longitudinal, shear and scalar spontaneous strain at 300°C, and constant *k* values for $La_{0.2}Nd_{0.2}Sm_{0.2}Gd_{0.2}RE5_{0.2}NbO_4$ (where RE5 = Ho, Y, Tb, Eu, Pr) series.

RE5	u (10^{-2})	v (10^{-2})	ε_s (10^{-2})	k
Ho	2.42	3.01	5.46	14.29
Y	2.43	3.02	5.48	13.57
Tb	2.48	3.03	5.57	13.14
Eu	2.53	3.04	5.59	13.30
Pr	2.58	2.98	5.57	13.92

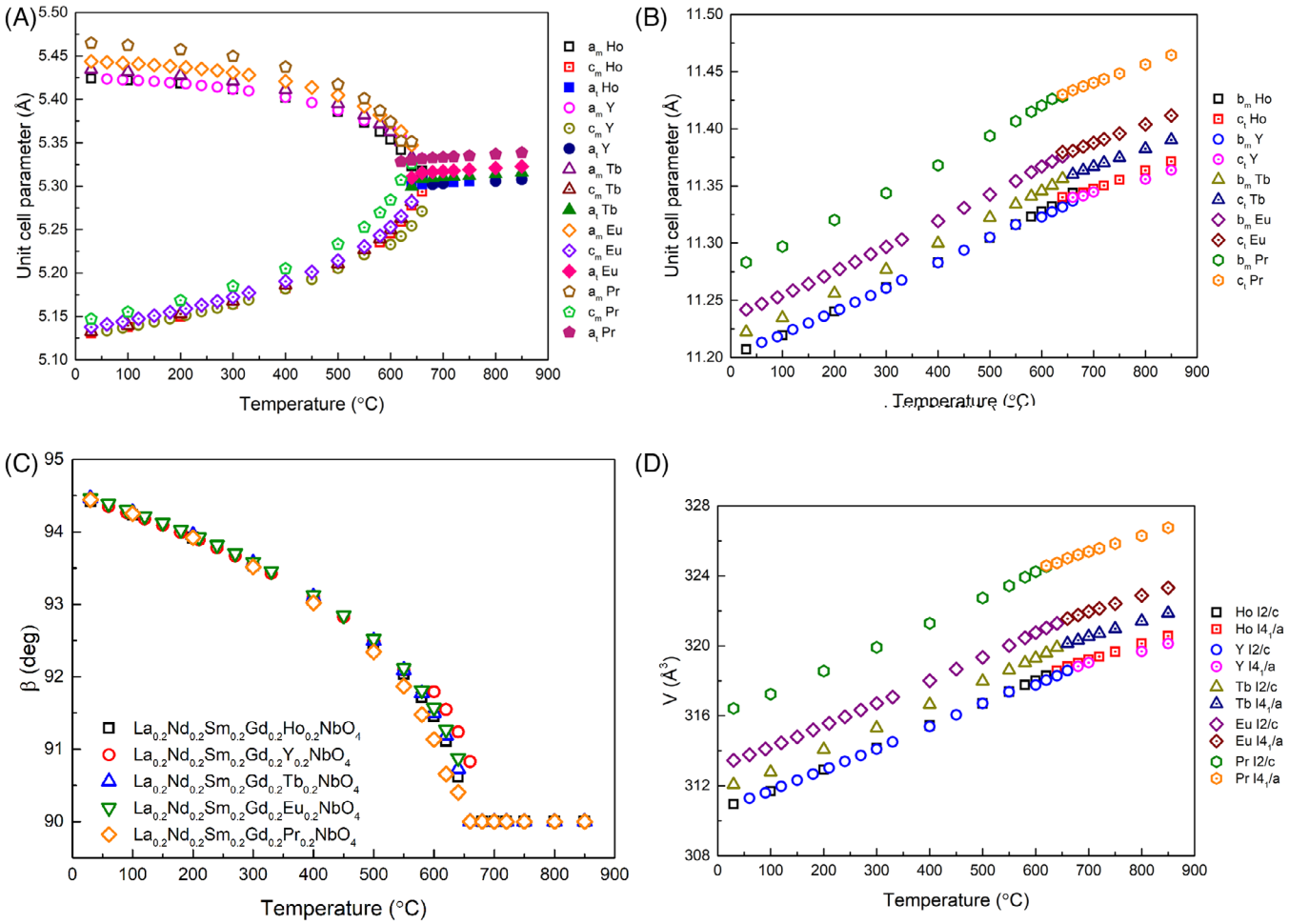

FIGURE 4 (A) Temperature-dependent evolution of unit cell parameters between monoclinic a_m and c_m and tetragonal a_t polymorphs of the $La_{0.2}Nd_{0.2}Sm_{0.2}Gd_{0.2}RE5_{0.2}NbO_4$ (RE5 = Ho, Y, Tb, Eu, Pr) series. Parameters related to monoclinic polymorph are denoted by open symbols (also with a dot), while tetragonal ones by filled symbols. (B) Temperature-dependent evolution of unit cell parameters between monoclinic b_m and tetragonal c_t polymorphs of the $La_{0.2}Nd_{0.2}Sm_{0.2}Gd_{0.2}RE5_{0.2}NbO_4$ (RE5 = Ho, Y, Tb, Eu, Pr) series. Parameters related to the monoclinic polymorph are denoted by open symbols, while tetragonal ones by open symbols filled with a dot. (C) Evolution of the monoclinic angle β with increasing temperature of the $La_{0.2}Nd_{0.2}Sm_{0.2}Gd_{0.2}RE5_{0.2}NbO_4$ (RE5 = Ho, Y, Tb, Eu, Pr) series. (D) Evolution of the unit cell volume with increasing temperature of the $La_{0.2}Nd_{0.2}Sm_{0.2}Gd_{0.2}RE5_{0.2}NbO_4$ (RE5 = Ho, Y, Tb, Eu, Pr) series. Volumes related to monoclinic polymorph are denoted by open symbols, while tetragonal ones by open symbols filled with a dot.

position of atoms and parameters of the unit cell, which seem to be continuous throughout the entire temperature range. Nevertheless, it should be remembered that there are also some indications of the first-order nature of this transition. For instance, Auckett et al.[40] have recently reported that in $LaNb_{1-x}Mo_xO_{4+0.5x}$ (x = 0, 0.08, 0.12, 0.16, and 0.20) series, the structural phase transition is of the first order. Based on the variable-temperature XRD tests, apart from a typical coexistence of the Fergusonite and Scheelite phases, they also observed the hysteresis in structural properties around the transition temperature.[40] That indicates the presence of an energy barrier associated with the transition meaning the first-order phase transition. With the density functional theory (DFT) calculations carried out for $LaNbO_4$, they found that the energy barrier is relatively low (below 0.207 eV per unit cell), which could explain why the transition is usually described as continuous second-order transition.[40] Indeed, our results support the second-order type of the structural transition, which may be illustrated by (Figure 6B) the relationship between the Landau order parameter and the spontaneous strain. In agreement with Equation (16), in the temperature range far from the transition, it is linear within the experimental error. The k values found for $La_{0.2}Nd_{0.2}Sm_{0.2}Gd_{0.2}RE5_{0.2}NbO_4$ (~14) are higher in comparison to those for the non-multicomponent orthoniobates which are, for example, 10.52 for $LaNbO_4$,[6] 11.2 for $La_{0.98}Mg_{0.02}NbO_{4-\delta}$,[37] and 9.1 for $LaNb_{0.4}Ta_{0.6}O_4$.[13] On the other hand, they were much lower than the k values reported for $LaNb_{0.85}Sb_{0.15}O_4$ (32.5[10]).

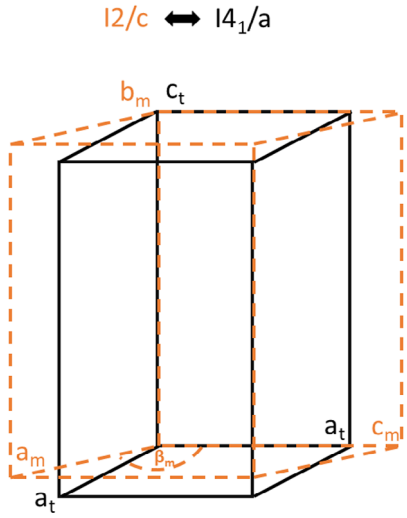

FIGURE 5 Transformation of unit cell parameters during the structural phase transition in lanthanum ortho-niobate.

TABLE 3 Thermal expansion coefficients and transition temperatures of the $La_{0.2}Nd_{0.2}Sm_{0.2}Gd_{0.2}RE5_{0.2}NbO_4$ (where RE5 = Ho, Y, Tb, Eu, and Pr).

	Thermal expansion coefficients (10^{-6} K^{-1})		T_0 (°C)	
RE5	Monoclinic phase	Tetragonal phase	Measurement	Average value
Ho	12.8 (2)	9.9 (1)	688 (15)	710
Y	12.8 (2)	9.9 (1)	686 (17)	710
Tb	12.7 (2)	9.8 (2)	701 (12)	706
Eu	12.9 (2)	9.8 (2)	690 (15)	712
Pr	13.2 (2)	9.7 (1)	676 (17)	686

Note: The numbers in parentheses represent half of the temperature range in which a step in the $\frac{d(\Delta L/L_0)}{dT}$ occurs.

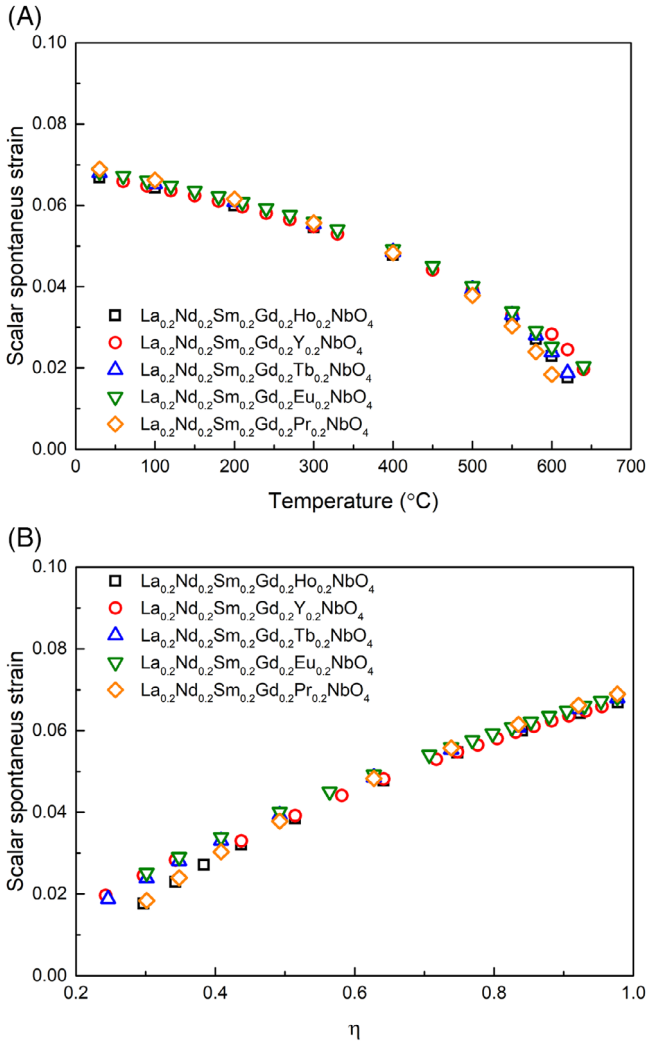

FIGURE 6 (A) Scalar spontaneous strain as a function of temperature for the $La_{0.2}Nd_{0.2}Sm_{0.2}Gd_{0.2}RE5_{0.2}NbO_4$ (RE5 = Ho, Y, Tb, Eu, Pr) series. (B) Relationship between the order parameter (η) and the magnitude of the spontaneous strain (ε_s). The symbols show the calculated scalar spontaneous strain for each composition.

3.3 | Dilatometry

Figure 7 depicts the relative elongation, $\Delta L/L_0$, of the $La_{0.2}Nd_{0.2}Sm_{0.2}Gd_{0.2}RE5_{0.2}NbO_4$ (where RE5 = Ho, Y, Tb, Eu, Pr) series as a function of the temperature. The temperature dependence of relative elongation in all samples shows distinct bending occur above 675°C. The temperature at which the slope changes can be thought of as the temperature of the phase transition between monoclinic (I2/c) and tetragonal (I4$_1$/a) structures.[6,11,37,41] The inset depicts the dependence of the $\frac{d(\Delta L/L_0)}{dT}$ as the function of the temperature of the samples, which corresponds to the linear TEC.[6] The results are shown in Table 3.

TECs of $La_{0.2}Nd_{0.2}Sm_{0.2}Gd_{0.2}RE5_{0.2}NbO_4$ in the monoclinic phase are similar or lower than those of undoped (15.3×10^{-6} K^{-1} and 14×10^{-6} K^{-1})[41,42] and acceptor-doped $LaNbO_4$ (between 12 and 18×10^{-6} K^{-1}).[42] On the other hand, the $La_{0.2}Nd_{0.2}Sm_{0.2}Gd_{0.2}RE5_{0.2}NbO_4$ TEC in the tetragonal phase (9.7– 9.9×10^{-6} K^{-1}) is significantly higher than in the other niobates in which it does not exceed 9.1×10^{-6} K^{-1}.[37,41,42] As discussed by Liu et al.,[43] in ABO_4 oxides TEC is related mostly to the A–O bond strength. This bond is predominantly ionic so its strength may be expected to increase with the decreasing electronegativity of the A-cation. The average A-cation Pauling electronegativities for the samples with Ho, Y, Eu, Tb, and Pr are 1.168, 1.166, 1.160, 1.160, and 1.148, respectively. This agrees well with the changes in TEC in the tetragonal phase, whereas the monoclinic TEC values do not show such a tendency.

Based on the curves shown in Figure 7, the phase transition temperatures (T_0) were determined by calculating the first derivatives from the plots. The phase transition temperatures are listed in Table 3. For comparison, the

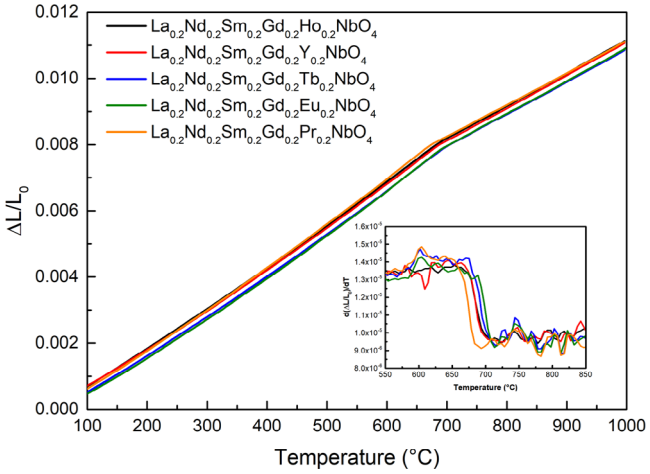

FIGURE 7 Relative elongation of the $La_{0.2}Nd_{0.2}Sm_{0.2}Gd_{0.2}Ho_{0.2}NbO_4$, $La_{0.2}Nd_{0.2}Sm_{0.2}Gd_{0.2}Y_{0.2}NbO_4$, $La_{0.2}Nd_{0.2}Sm_{0.2}Gd_{0.2}Tb_{0.2}NbO_4$, $La_{0.2}Nd_{0.2}Sm_{0.2}Gd_{0.2}Eu_{0.2}NbO_4$, and $La_{0.2}Nd_{0.2}Sm_{0.2}Gd_{0.2}Pr_{0.2}NbO_4$ samples as a function of the temperature recorded during cooling. The temperature derivatives around the phase transition region temperature of all samples are shown in the inset.

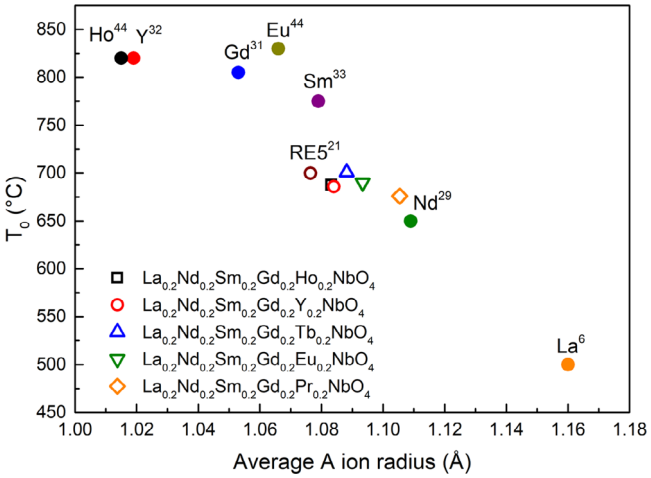

FIGURE 8 The temperature of phase transition as a function of the A-cation average ionic radius of $La_{0.2}Nd_{0.2}Sm_{0.2}Gd_{0.2}Ho_{0.2}NbO_4$, $La_{0.2}Nd_{0.2}Sm_{0.2}Gd_{0.2}Y_{0.2}NbO_4$, $La_{0.2}Nd_{0.2}Sm_{0.2}Gd_{0.2}Tb_{0.2}NbO_4$, $La_{0.2}Nd_{0.2}Sm_{0.2}Gd_{0.2}Eu_{0.2}NbO_4$, and $La_{0.2}Nd_{0.2}Sm_{0.2}Gd_{0.2}Pr_{0.2}NbO_4$ (hollow marks) as well as for $La_{1/5}Nd_{1/5}Sm_{1/5}Ho_{1/5}Y_{1/5}NbO_4$[21] (RE5NbO$_4$). For comparison, the data for LaNbO$_4$,[6] NdNbO$_4$,[29] SmNbO$_4$,[33] GdNbO$_4$,[31] HoNbO$_4$,[44] YNbO$_4$,[32] and EuNbO$_4$[44] were added (filled symbols).

calculated average values of the structural phase transition temperatures based on La-, Nd-, Sm-, Gd-, Ho-, Y-, Tb-, Eu-, and PrNbO$_4$ are also shown. Transition temperatures vary from 676°C to 701°C, which is similar to the phase transition temperature ranges determined based on the high-temperature XRD. The transition temperatures of the $La_{0.2}Nd_{0.2}Sm_{0.2}Gd_{0.2}RE5_{0.2}NbO_4$ (where RE5 = Ho, Y, Tb, Eu and Pr) series are a little lower than the average values of the transition temperatures for LaNbO$_4$ (500°C[6]), NdNbO$_4$ (650°C[29]), SmNbO$_4$ (775°C[33]), GdNbO$_4$ (805°C[31]), HoNbO$_4$ (820°C[44]), YNbO$_4$ (820°C[32]), TbNbO$_4$ (800°C[45]), EuNbO$_4$ (830°C[44]), and PrNbO$_4$ (700°C[46]). It is consistent with a lower monoclinic angle shown by the multicomponent oxides. Figure 8 shows the structural phase transition temperatures of the $La_{0.2}Nd_{0.2}Sm_{0.2}Gd_{0.2}Ho_{0.2}NbO_4$, $La_{0.2}Nd_{0.2}Sm_{0.2}Gd_{0.2}Y_{0.2}NbO_4$, $La_{0.2}Nd_{0.2}Sm_{0.2}Gd_{0.2}Tb_{0.2}NbO_4$, $La_{0.2}Nd_{0.2}Sm_{0.2}Gd_{0.2}Eu_{0.2}NbO_4$, and $La_{0.2}Nd_{0.2}Sm_{0.2}Gd_{0.2}Pr_{0.2}NbO_4$ samples as a function of average A-site ion radius. For comparison, the phase transition temperatures of LaNbO$_4$, NdNbO$_4$, SmNbO$_4$, GdNbO$_4$, HoNbO$_4$, YNbO$_4$, EuNbO$_4$, and $La_{1/5}Nd_{1/5}Sm_{1/5}Ho_{1/5}Y_{1/5}NbO_4$ are also added. The discussion regarding the nature and the mechanism of the Fergusonite–Scheelite phase transition as well as the factors influencing the transition temperature have not been concluded yet. A step-like increase in the temperature expansion coefficient shown in the inset of Figure 7 supports the idea that it is a second-order phase transition. The structural changes occurring in the transition involve distortion of the NbO$_4$ tetrahedra,[32] which means that the changes in the A-cations have a weaker influence on the transition temperature than those in the B-cations. Nevertheless, it can be seen that in both the conventional and multicomponent rare-earth ortho-niobates the phase transition temperature decreases as the ionic radius of lanthanides increases (filled symbols). In the case of multicomponent rare-earth ortho-niobates, the influence of the A-cation radius is much weaker. Similarly, weak influence of ionic radius on T_0 was observed in our recent work regarding $La_{1/5}Nd_{1/5}Sm_{1/5}Gd_{1/5}Eu_{1/5}NbO_4$, $La_{1/6}Nd_{1/6}Sm_{1/6}Gd_{1/6}Eu_{1/6}Ho_{1/6}NbO_4$, and $La_{1/7}Nd_{1/7}Sm_{1/7}Gd_{1/7}Eu_{1/7}Ho_{1/7}Er_{1/7}NbO_4$ oxides.[47] We propose that the local disorder in the neighborhood of the A–O bonds influences the ability of the NbO$_4$ tetrahedra to distort. Therefore, it may affect both the transition temperature and the temperature range of the coexistence of the monoclinic and tetragonal phases.

4 | CONCLUSIONS

Multicomponent rare-earth ortho-niobates in the series of $La_{0.2}Nd_{0.2}Sm_{0.2}Gd_{0.2}RE5_{0.2}NbO_4$ (where RE5 = Ho, Y, Tb, Eu, and Pr) were synthesized via solid-state reaction route. These materials are stable at room temperature in the monoclinic I2/c structure and are pure single-phase, according to structural studies performed with synchrotron radiation (SR-XRD).

High-temperature X-ray powder diffraction and dilatometry studies have shown that in multicomponent

rare-earth ortho-niobates, a structural phase transition occurs. The transition temperatures ranged from 676°C to 701°C. The structural phase transition temperatures of multicomponent oxides similarly to conventional ones decrease with increasing ionic radius of the A-cation. Based on the observed relation between the Landau order parameter and spontaneous strain, the transition has been classified as a second-order phase transition. In every composition, the coexistence of the monoclinic and tetragonal phases has been observed close to the structural phase transition temperature.

The presence of two orientation states in the monoclinic structure leads to the so-called spontaneous strain, which consists of longitudinal (u) and shear (v) strain components. The values of these strains at 300°C range between 2.42 and 2.58 $\times 10^{-2}$ for longitudinal, 2.98 and 3.04 $\times 10^{-2}$ for shear, and 5.46 and 5.57 $\times 10^{-2}$ for scalar spontaneous strain. The components of strain increase with increasing average radius of the A ion except for $La_{0.2}Nd_{0.2}Sm_{0.2}Gd_{0.2}Pr_{0.2}NbO_4$ in which higher shear strain was observed. This may be due to oxygen absorption and desorption.

It was noticed that the difference in the complexity of the composition of the A sublattice had a small impact on the spontaneous strain in all the tested materials.

ACKNOWLEDGMENTS

This research was supported by the National Science Centre Poland under the OPUS scheme "High-entropy oxides for energy conversion" (ref. no. 2019/35/B/ST5/00888). The authors acknowledge the CERIC-ERIC Consortium (Grant/Award Number: 2021202) for the access to experimental facilities. We acknowledge Elettra Sincrotrone Trieste for providing access to its synchrotron radiation facilities and we thank Jasper Rikkert Plaisier for assistance in using beamline MCX.

ORCID

Arkadiusz Dawczak https://orcid.org/0000-0002-7880-7627
Aleksandra Mielewczyk-Gryń https://orcid.org/0000-0001-6795-3840
Maria Gazda https://orcid.org/0000-0001-6193-7815

REFERENCES

1. Duan C, Huang J, Sullivan N, O'Hayre R. Proton-conducting oxides for energy conversion and storage. Appl Phys Rev. 2020;7:011314.
2. Kim J, Sengodan S, Kim S, Kwon O, Bu Y, Kim G. Proton conducting oxides: a review of materials and applications for renewable energy conversion and storage. Renew Sustain Energy Rev. 2019;109:606–18.
3. Malavasi L, Fisher CAJ, Islam MS. Oxide-ion and proton conducting electrolyte materials for clean energy applications: structural and mechanistic features. Chem Soc Rev. 2010;39:4370–87.
4. Norby T, Magrasó A. On the development of proton ceramic fuel cells based on Ca-doped $LaNbO_4$ as electrolyte. J Power Sources. 2015;282:28–33.
5. Kochetova N, Animitsa I, Medvedev D, Demin A, Tsiakaras P. Recent activity in the development of proton-conducting oxides for high-temperature applications. RSC Adv. 2016;6:73222–68.
6. Jian L, Wayman CM. Monoclinic-to-tetragonal phase transformation in a ceramic rare-earth orthoniobate, $LaNbO_4$. J Am Ceram Soc. 1997;80:803–6.
7. Mielewczyk-Gryń A, Wachowski S, Prześniak-Welenc M, Dzierzgowski K, Regoutz A, Payne DJ, et al. Water uptake analysis of acceptor-doped lanthanum orthoniobates. J Therm Anal Calorim. 2019;138:225–32.
8. Haugsrud R, Norby T. Proton conduction in rare-earth ortho-niobates and ortho-tantalates. Nat Mater. 2006;5:193–96.
9. Haugsrud R, Norby T. High-temperature proton conductivity in acceptor-doped $LaNbO_4$. Solid State Ion. 2006;177:1129–35.
10. Mielewczyk-Gryn A, Wachowski S, Lilova K, Guo X, Gazda M, Navrotsky A. Influence of antimony substitution on spontaneous strain and thermodynamic stability of lanthanum orthoniobate. Ceram Int. 2015;41:2128–33.
11. Wachowski S, Mielewczyk-Gryn A, Gazda M. Effect of isovalent substitution on microstructure and phase transition of $LaNb_{1-x}M_xO_4$ (M = Sb, V or Ta; $x = 0.05–0.3$). J Solid State Chem. 2014;219:201–9.
12. Wachowski S, Kamecki B, Winiarz P, Dzierzgowski K, Mielewczyk-Gryń A, Gazda M. Tailoring structural properties of lanthanum orthoniobates through an isovalent substitution on the Nb-site. Inorg Chem Front. 2018;5:2157–66.
13. Vullum F, Nitsche F, Selbach SM, Grande T. Solid solubility and phase transitions in the system $LaNb_{1-x}Ta_xO_4$. J Solid State Chem. 2008;181:2580–85.
14. Yeh JW, Chen S-K, Lin S-J, Gan J-Y, Chin T-S, Shun T-T, et al. Nanostructured high-entropy alloys with multiple principal elements: novel alloy design concepts and outcomes. Adv Eng Mater. 2004;6:299–303.
15. Rost CM, Sachet E, Borman T, Moballegh A, Dickey EC, Hou D, et al. Entropy-stabilized oxides. Nat Commun. 2015;6:8485.
16. Amiri A, Shahbazian-Yassar R. Recent progress of high-entropy materials for energy storage and conversion. J Mater Chem A Mater. 2021;9:782–823.
17. Sarkar A, Velasco L, Wang D, Wang Q, Talasila G, Biasi L, et al. High entropy oxides for reversible energy storage. Nat Commun. 2018;9:3400.
18. Gazda M, Miruszewski T, Jaworski D, Mielewczyk-Gryń A, Skubida W, Wachowski S, et al. Novel class of proton conducting materials—high entropy oxides. ACS Mater Lett. 2020;2:1315–21.
19. Zhu J, Xu J, Zhang P, Meng X, Cao S, Wu J-M, et al. Enhanced mechanical and thermal properties of ferroelastic high-entropy rare-earth-niobates. Scr Mater. 2021;200:113912.
20. Dawczak A, Skubida W, Mielewczyk-Gryń A, Gazda M. Enhanced acceptor concentration, proton conductivity, and hydration in multicomponent rare-earth ortho-niobates. J Am Ceram Soc. 2023;107(1):253–64. https://doi.org/10.1111/jace.19440

21. Chen D, Yan N, Cao X, Li F, Liu L, Shen Q, et al. Entropy regulation in $LaNbO_4$-based Fergusonite to implement high-temperature phase transition and promising dielectric properties. J Adv Ceram. 2023;12:1067–80.
22. Toby BH. R factors in Rietveld analysis: how good is good enough? Powder Diffr. 2006;21:67–70.
23. Toby BH, Von Dreele RB. GSAS-II: the genesis of a modern open-source all purpose crystallography software package. J Appl Crystallogr. 2013;46:544–49.
24. Momma K, Izumi F. VESTA 3 for three-dimensional visualization of crystal, volumetric and morphology data. J Appl Crystallogr. 2011;44:1272–76.
25. Fjeld H, Toyoura K, Haugsrud R, Norby T. Proton mobility through a second order phase transition: theoretical and experimental study of $LaNbO_4$. Phys Chem Chem Phys. 2010;12:10313–19.
26. Aizu K. Determination of the state parameters and formulation of spontaneous strain for ferroelastics. J Phys Soc Jpn. 1970;28:706–16.
27. Schlenker JL, Gibbs GV, Boisen MB. Strain-tensor components expressed in terms of lattice parameters. Acta Crystallogr Sect A. 1978;34:52–54.
28. Dzierzgowski K, Wachowski S, Gazda M, Mielewczyk-Gryń A. Terbium substituted lanthanum orthoniobate: electrical and structural properties. Crystals (Basel). 2019;9:1–14.
29. Saura-Múzquiz M, Mullens BG, Maynard-Casely HE, Kennedy BJ. Neutron diffraction study of the monoclinic-tetragonal phase transition in $NdNbO_4$ and $NdTaO_4$. Dalton Trans. 2021;50:11485–97.
30. Mullens BG, Avdeev M, Brand HEA, Mondal S, Vaitheeswaran G, Kennedy BJ, et al. Insights into the structural variations in $SmNb_{1-x}Ta_xO_4$ and $HoNb_{1-x}Ta_xO_4$ combined experimental and computational studies. Dalton Trans. 2021;50:9103–17.
31. Kondrat'eva ON, Nikiforova GE, Tyurin AV, Khoroshilov AV, Gurevich VM, Gavrichev KS, et al. Thermodynamic properties of, and Fergusonite-to-Scheelite phase transition in, gadolinium orthoniobate $GdNbO_4$ ceramics. J Alloys Compd. 2019;779:660–66.
32. Sarin P, Hughes RW, Lowry DR, Apostolov ZD, Kriven WM. High-temperature properties and ferroelastic phase transitions in rare-earth niobates ($LnNbO_4$). J Am Ceram Soc. 2014;97:3307–19.
33. Arulnesan SW, Kayser P, Kimpton JA, Kennedy BJ. Studies of the Fergusonite to Scheelite phase transition in $LnNbO_4$ orthoniobates. J Solid State Chem. 2019;277:229–39.
34. Liu L, Chen Y, Feng Z, Wu H, Zhang X. Crystal structure, infrared spectra, and microwave dielectric properties of the $EuNbO_4$ ceramic. Ceram Int. 2021;47:4321–26.
35. Peixoto JC, Dias A, Matinaga FM, Siqueira KPF. Luminescence properties of $PrNbO_4$ and $EuNbO_4$ orthoniobates and investigation of their structural phase transition by high-temperature Raman spectroscopy. J Lumin. 2021;238:118284.
36. Shannon RD. Revised effective ionic radii and systematic studies of interatomic distances in halides and chalcogenides. Acta Crystallogr Sect A. 1976;32:751–67.
37. Mielewczyk-Gryn A, Gdula-Kasica K, Kusz B, Gazda M. High temperature monoclinic-to-tetragonal phase transition in magnesium doped lanthanum ortho-niobate. Ceram Int. 2013;39:4239–44.
38. Niu G, Zoellner MH, Schroeder T, Schaefer A, Jhang J-H., Zielasek V, et al. Controlling the physics and chemistry of binary and ternary praseodymium and cerium oxide systems. Phys Chem Chem Phys. 2015;17:24513–40.
39. Takasu Y, Matsui M, Tamura H, Kawamura S, Matsuda Y, Toyoshima I. Temperature-programmed desorption on the unstable lattice oxygen of praseodymium oxide. J Catal. 1981;69:51–57.
40. Auckett JE, Lopez-Odriozola L, Clark SJ, Evans IR. Exploring the nature of the Fergusonite–Scheelite phase transition and ionic conductivity enhancement by Mo^{6+} doping in $LaNbO_4$. J Mater Chem A Mater. 2021;9:4091–102.
41. Huse M, Skilbred AWB, Karlsson M, Eriksson S, Norby T, Haugsrud R, et al. Neutron diffraction study of the monoclinic to tetragonal structural transition in $LaNbO_4$ and its relation to proton mobility. J Solid State Chem. 2012;187:27–34.
42. Mokkelbost T, Lein HL, Vullum PE, Holmestad R, Grande T, Einarsrud M-A. Thermal and mechanical properties of $LaNbO_4$-based ceramics. Ceram Int. 2009;35:2877–83.
43. Liu T, Zhang X, Guan J, Catlow CRA, Walsh A, Sokol AA, et al. Insight into the Fergusonite–Scheelite phase transition of ABO_4-type oxides by density functional theory: a case study of the subtleties of the ground state of $BiVO_4$. Chem Mater. 2022;34:5334–43.
44. Kukueva LL, Ivanova LA, Venevtsev YN. Ferroelastics with the Fergusonite type structure. Ferroelectrics. 1984;55:129–33.
45. Dzierzgowski K. Właściwości i Struktura Niobianu Lantanu Domieszkowanego Pierwiastkami Ziem Rzadkich. 2021.
46. Dzierzgowski K, Wachowski S, Łapiński M, Mielewczyk-Gryń A, Gazda M. Praseodymium orthoniobate and praseodymium substituted lanthanum orthoniobate: electrical and structural properties. Materials. 2022;15:1–20.
47. Elameen AAA, Dawczak A, Miruszewski T, Gazda M, Wachowski S. Proton conductivity in multi-component ABO_4-type oxides. Phys Chem Chem Phys. 2023;25:29127–34.

SUPPORTING INFORMATION

Additional supporting information can be found online in the Supporting Information section at the end of this article.

How to cite this article: Dawczak A, Mielewczyk-Gryń A, Gazda M. Structural phase transitions in multicomponent $La_{0.2}Nd_{0.2}Sm_{0.2}Gd_{0.2}RE5_{0.2}NbO_4$ (RE5 = Ho, Y, Tb, Eu, Pr) oxides. J Am Ceram Soc. 2024;1–11. https://doi.org/10.1111/jace.19942